Journal of Applied Physics

Analytic Wigner distribution function for tunneling and trajectory models

Cite as: J. Appl. Phys. **125**, 114303 (2019); https://doi.org/10.1063/1.5086434
Submitted: 20 December 2018 . Accepted: 22 February 2019 . Published Online: 19 March 2019

K. L. Jensen, D. A. Shiffler, J. L. Lebowitz, M. Cahay, and J. J. Petillo

Journal of Applied Physics ARTICLE scitation.org/journal/jap

Analytic Wigner distribution function for tunneling and trajectory models

Cite as: J. Appl. Phys. **125**, 114303 (2019); doi: 10.1063/1.5086434
Submitted: 20 December 2018 · Accepted: 22 February 2019 ·
Published Online: 19 March 2019

K. L. Jensen,[1] D. A. Shiffler,[2] J. L. Lebowitz,[3] M. Cahay,[4] and J. J. Petillo[5]

AFFILIATIONS

[1]Code 6362, MSTD, Naval Research Laboratory, Washington, DC 20375, USA
[2]Directed Energy Directorate, Air Force Research Laboratory, Albuquerque, New Mexico 87117, USA
[3]Center for Mathematical Sciences Research, Rutgers University, Piscataway, New Jersey 08854, USA
[4]Department of Electrical Engineering and Computer Science, University of Cincinnati, Cincinnati, Ohio 45221, USA
[5]Center for Electromagnetics, DEOST, Leidos, Billerica, Massachusetts 01821, USA

ABSTRACT

The Wigner function is assembled from analytic wave functions for a one-dimensional closed system (well with infinite barriers). A sudden change in the boundary potentials allows for the investigation of time-dependent effects in an analytically solvable model. A trajectory model is developed to account for tunneling when the barrier is finite. The behavior of the density (the zeroth moment of the Wigner function) after an abrupt change in potential shows net accumulation and depletion over time for a weighting of energy levels characteristic of the supply function in field emission. However, for a closed system, the methods have application to investigations of tunneling and transmission associated with field and photoemission at short time scales.

https://doi.org/10.1063/1.5086434

I. INTRODUCTION

Models of phenomena in narrow anode-cathode gaps are of increasing importance in nanoscale studies treating quantum tunneling and time dependent behavior for field and photoemission.[1–7] When anode-cathode gaps are comparable to tunneling distances, or when emitter curvature is such that changes to the tunneling path result in departures from conventional treatments, then the reliability of those approaches, which lead to the 1D equations of electron emission, is affected.[8–12] The canonical equations are based on the evaluation of transmission and reflection coefficients and probabilities, which are standard problems in quantum mechanics[13–15] for the evaluation of current, but the problem of tunneling time remains unresolved,[16–19] more so for curved tunneling paths. A trajectory interpretation is desirable to develop to model emission at very short time scales and accounts for how tunneling and complications such as multidimensionality[7,20] are to be addressed. Additionally, a trajectory interpretation would allow tunneling time contributions to be associated with delayed emission effects in the prediction of emission pulse properties.[21] Before a trajectory interpretation can be realized, however, methods to reconcile quantum mechanics with classical trajectory-like behavior are required. Wigner[22–24] and Bohm trajectories (or "paths")[25–29] have properties that may be appropriate. Numerical simulations of resonant tunneling diodes (RTDs) using the Wigner function,[30–33] for example, share similarities to how they are to be used here.

A suitable method is based on wave functions confined by Dirac delta function potentials $V(x) = \Gamma\delta(x)$, where Γ governs the strength of the potential,[34] as it provides a basis for finding a tractable Wigner distribution function (WDF). The wave function approach allows for treating time dependent behavior. The WDF allows for developing a trajectory interpretation. With modifications, the solutions can enable investigating field penetration effects into a barrier and responses to sudden changes in barrier height (as would accompany the sudden application of an applied field). The demonstration is undertaken with the simplest potential profiles first so as to develop the methods systematically: the first undertaking is a direct solution of Schrödinger's equation, and the second is based on a limiting procedure applied to a Transfer Matrix Approach (TMA)[35] for a potential modeled by a delta sequence.[36] The associated Wigner trajectories can then be developed. Finally, the time-dependent behavior of the wave functions after a sudden change in the potential is shown. These separately established components will be used to develop time dependent trajectories and their associated transit times in a separate study.

A. Schrödinger formulation

The stationary one-dimensional (1D) Schrödinger's equation for a Dirac delta function potential with $\Gamma \equiv \hbar^2\gamma/2m$ becomes

$$\partial_x^2\psi(x) = \{\gamma\delta(x) - k^2\}\psi(x). \tag{1}$$

Solutions are [where subscript a refers to the region to the left ($x < 0$) of the origin and b to the right ($x > 0$)]

$$\begin{aligned}\psi(x<0) \equiv \psi_a(x) &= Ae^{ikx} + Be^{-ikx},\\ \psi(x>0) \equiv \psi_b(x) &= A'e^{ikx} + B'e^{-ikx}.\end{aligned} \tag{2}$$

The conventional narrative, which treats an open system and thereby relates transmission and reflection probabilities, is now modified to consider a box with infinite barriers at $x = \pm L/2$ with a δ-function potential at the origin: such a system is closed (no current J) and has discrete energy levels. Although having $J = 0$ appears to be a limitation, it enables certain simplifications. The following conditions are then used to determine the coefficients of Eq. (2).

1. The continuity of $\psi(x)$ at $x = 0$ gives

$$A + B = A' + B'. \tag{3}$$

2. Being in a box requires current density $J_k(x) \equiv (\hbar/2mi)\left(\psi^\dagger\partial_x\psi - \psi\partial_x\psi^\dagger\right) = 0$ from which

$$|A|^2 - |B|^2 = |A'|^2 - |B'|^2 = 0 \tag{4}$$

and is satisfied by

$$B = Ae^{i\phi}, \quad B' = A'e^{i\varphi'}. \tag{5}$$

3. The boundaries $\psi_a(-L/2) = \psi_b(L/2) = 0$ entail

$$\phi = -kL + \pi, \quad \phi' = kL + \pi. \tag{6}$$

4. Integrating Schrödinger's equation from $x = 0^-$ to $x = 0^+$ results in $\partial_x\psi_b(0^+) - \partial_x\psi_a(0^-) = \gamma\psi_b(0)$, or

$$-A + A' + B - B' = -\frac{i\gamma}{k}(A' + B'), \tag{7}$$

which, using Conditions 2 and 3, becomes

$$(2k + i\gamma)e^{-ikL} + (-2k + i\gamma)e^{ikL} - 2i\gamma = 0. \tag{8}$$

5. The boundary conditions further entail even and odd parity solutions.
   - Even occurs for $k_j = \pi(2j+1)/L$ for which $\psi_a(x) = 2A\cos(k_jx)$ and $\psi_b(x) = 2A'\cos(k_jx)$, but then Eq. (8) requires $-4i\gamma = 0$, or the absence of a δ-function potential.
   - Odd occurs for $k_j = 2\pi j/L$ for which $\psi_a(x) = 2Ai\sin(k_jx)$ and $\psi_b(x) = 2A'i\sin(k_jx)$, but then Eq. (8) is identically zero and so odd parity solutions exist for any γ, because the wave function identically vanishes at $x = 0$.
6. If the wave function vanishes at the origin where the delta function exists, then the requirement that the derivative of the wave function be continuous entails $A = A'$.

The six conditions result in

$$\psi_a(x) = \psi_b(x) = 2\sin(k_jx), \tag{9}$$

where the normalization is over the cell size ($L/2$).

Importantly, the sequence of the derivation shows that increasing the box by $L \to 2L$ and inserting δ-function potentials at $\pm L/2$ (thereby excluding the "even parity" solutions) do not change the form of $\psi(x)$ but simply extends the range over which it holds to $\pm 3L/2$. The insertion of additional cells can therefore be iterated so that $L \to (N+1)L$ with N an integer and δ-function potentials placed at $x_p = pL/2$ with $p = 0, \pm 1, \pm 2, \ldots, \pm N$. When the even parity solutions of Condition 5 are excluded, then if A_j is associated with cell j, A_j need not be related [the wave function $\psi_j(x)$ for cell j is not affected by $\psi_{j\pm1}(x)$ for the adjacent cells]. When the even parity solutions *not* excluded, then the condition $\partial_x\psi(pL^+/2) - \partial_x\psi(pL^-/2) = \gamma\psi(pL/2)$ would have had to be accounted for, with $L^\pm$ being infinitesimally to the right or left of L.

B. Transfer Matrix Approach

The same result using a Transfer Matrix Approach (TMA) is now shown. The TMA allows for generalization to barriers with finite height and width and will therefore be applicable to barriers closer to conditions characteristic of field and photoemission. The Dirac delta function potential is replaced by a *delta sequence*[36] defined by

$$\delta_l(x) \equiv \frac{1}{l}\Theta\left[\left(\frac{l}{2}\right)^2 - x^2\right], \tag{10}$$

where $\Theta(z)$ is the Heaviside Step function (0 when $z < 0$, 1 when $z > 0$). It mimics a Delta function because (i) in the limit that $l \to 0$, then $\delta_l(x)$ is zero everywhere except at $x = 0$ where it goes to ∞ as $1/l$; (ii) the integral $\int_{-\infty}^{\infty}\delta_l(x)dx = 1$; and (iii) $\int_{-\infty}^{\infty} g(x)\delta_l(x)dx \approx g(0)$ for a smooth function $g(x)$ as l vanishes.

The formulation allows the use of plane wave solutions $e^{\pm ikx}$ for the wave function $\psi(x)$ in the regions to either side of the delta function barrier $\gamma\delta_l(x)$, and $e^{\pm\kappa x}$ in the thin region defining the barrier, where $\kappa^2 \equiv k_o^2 - k^2$, $\hbar^2k_o^2/2m = \gamma/l$ and $\hbar^2k^2/2m = E$.

A box of width L centered on the origin now possesses three regions. Let region 1 be defined by $-L/2 \le x < l/2$, region 2 by $-l/2 \le x \le l/2$, and region 3 by $l/2 < x \le L/2$. The wave functions given by $\psi_j(x) \equiv A_je^{ikx} + B_je^{-ikx}$ for $j = (1, 3)$ and $\psi_2(x) \equiv A_2e^{\kappa x} + B_2e^{-\kappa x}$, and their first derivatives, have to match

at $x = \pm l/2$, conditions which are expressed for $x = -l/2$ by

$$\begin{bmatrix} 1/P & P \\ ik/P & -ikP \end{bmatrix}\begin{bmatrix} A_1 \\ B_1 \end{bmatrix} = \begin{bmatrix} 1/T & T \\ \kappa/T & -\kappa T \end{bmatrix}\begin{bmatrix} A_2 \\ B_2 \end{bmatrix}, \tag{11}$$

where $P(x = l/2) = e^{ikl/2}$ and $T(x = l/2) = e^{\kappa l/2}$, and for $x = l/2$ by

$$\begin{bmatrix} T & 1/T \\ \kappa T & -\kappa/T \end{bmatrix}\begin{bmatrix} A_2 \\ B_2 \end{bmatrix} = \begin{bmatrix} P & 1/P \\ ikP & -ik/P \end{bmatrix}\begin{bmatrix} A_3 \\ B_3 \end{bmatrix}. \tag{12}$$

Boundary conditions are a consequence of walls where $V(\pm L/2) = \infty$, for which the wave functions vanish $[\psi_1(-L/2) = \psi_3(L/2) = 0]$, or

$$(A_1 + B_1)\cos(Lk/2) - i(A_1 - B_1)\sin(Lk/2) = 0, \tag{13}$$

$$(A_3 + B_3)\cos(Lk/2) + i(A_3 - B_3)\sin(Lk/2) = 0, \tag{14}$$

where Eqs. (13) and (14) are used to specify the energy levels $k \to k_n$: when $A_j = -B_j$, then $k_n = 2\pi nx/L$, whereas when $A_j = B_j$, then $k_n = \pi(2n-1)x/L$. Eliminate A_2 and B_2 to obtain

$$\begin{bmatrix} A_3 \\ B_3 \end{bmatrix} = \begin{bmatrix} -(R/2\kappa k)e^{-ikl} & -iS \\ iS & -(R^\dagger/2\kappa k)e^{-ikl} \end{bmatrix}\begin{bmatrix} A_1 \\ B_1 \end{bmatrix}, \tag{15}$$

where

$$\begin{aligned} R &= -2\kappa k\cosh(\kappa l) + i(\kappa^2 - k^2)\sinh(\kappa l), \\ S &= \frac{\kappa^2 + k^2}{2\kappa k}\sinh(\kappa l) \end{aligned} \tag{16}$$

and where $\kappa^2 = k_o^2 - k^2$. In the limit of small barrier width $l \ll L$ and large barrier height $(k_o \gg k)$, a parameter a is introduced such that $l = La^2$ and $k_o = \sqrt{\gamma/l} = (\gamma/L)^{1/2}a^{-1}$. For small a, then,

$$\begin{aligned} R &\approx \kappa(-2k + i\gamma)(1 + ikLa^2), \\ S &\approx \frac{\gamma}{2k}. \end{aligned} \tag{17}$$

As a result, to order a^3

$$\begin{bmatrix} A_3 \\ B_3 \end{bmatrix} = \frac{1}{2k}\begin{bmatrix} 2k - i\gamma & -i\gamma \\ i\gamma & 2k + i\gamma \end{bmatrix}\begin{bmatrix} A_1 \\ B_1 \end{bmatrix}. \tag{18}$$

Consequently, in the limit $a \to 0$, when $B_j = -A_j$ for $j = 1, 3$, then $k_n = 2\pi n/L$ and $\psi \propto \sin(k_n x)$ for any value of γ; however, when $B_j = A_j$ then $k = \pi(2n-1)/L$ and $\psi_j \propto \cos(k_n x)$ only for $\gamma = 0$. The presence of a delta-function potential, therefore, entails only sine forms of the wave function for the closed system under consideration (for open boundary conditions, the cosine wave functions have to be retained).

II. WELL AND INFINITE BARRIERS

A. Density matrix

A wave function contained in a region with infinite barrier walls but otherwise such that $V(0 \le x \le L/2) = 0$ is of the form $\psi_n(x) \sim \sin(k_n x)$ with $k_n = 2\pi nx/L$, as occurs for either a well of width $L/2$ or one cell of a well with a delta function potential at the origin. Then, letting $|A_n|^2$ be proportional to the probability of being in a state ψ_n, the density $\rho(x)$ is given by

$$\rho(x) = \frac{2}{L}\sum_{n=1}^{N} A_n^2\left[\sin\left(\frac{2\pi nx}{L}\right)\right]^2, \tag{19}$$

where the normalized wave functions are given by $\psi_n(x) = \sqrt{2/L}\sin(k_n x)$ (compare Ref. 37, which applies the formalism to Wigner wave packets). Since separate regions are no longer under discussion here, but different wave functions are, the subscript in A_n is associated with k_n. If A_n^2 mimics $f(k)$ from Eq. (A1), then

$$\frac{\rho(x)}{\rho_o} = \frac{3}{N^3}\sum_{n=1}^{N}(N^2 - n^2)[\sin(2\pi nx/L)]^2 \tag{20}$$

as illustrated for various values of n in Fig. 1, where $k_N \equiv k_F$ is the energy of the highest filled level and corresponds to $k_F = \sqrt{2m\mu}/\hbar$, where μ is the chemical potential (or the Fermi level at $T = 0$ K). Adopting the notation $\psi_n(x) \equiv \langle k_n|x\rangle$, then Eq. (19) becomes the diagonal elements of a mixed density matrix, or

$$\rho(x) = \sum_{n=1}^{N} f(k_n)|\langle k_n|x\rangle|^2 = \langle x|\hat{\rho}|x\rangle, \tag{21}$$

where the density matrix $\hat{\rho}$ is defined by

$$\hat{\rho} \equiv \sum_{n=1}^{N} f_n|n\rangle\langle n|, \tag{22}$$

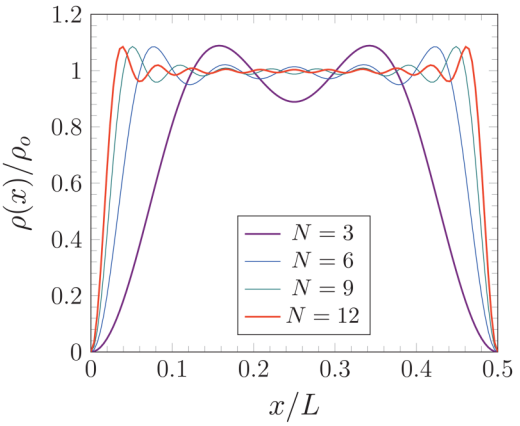

FIG. 1. $\rho(x)/\rho_o$ for $N \in (3, 6, 9, 12)$ as per Eq. (20). The (symmetrical) $x < 0$ region is not shown. Compare to Fig. 12. Note that the number of "humps" is given by $(n - 1)$.

where $|k_n\rangle \to |n\rangle$ to reinforce that $|k_n\rangle$ is not the same as the $|k\rangle$ momentum basis states often encountered. The weighting factor f_n takes over the role of A_j^2 and eases its identification with the supply function of Eq. (A1).

B. Wigner function

The Wigner distribution function (WDF) is obtained from the density matrix $\hat{\rho}$ by[38,39]

$$f(x,k) \equiv \frac{1}{\pi}\int_{-\infty}^{\infty} dy\, e^{2iky}\langle x-y|\hat{\rho}|x+y\rangle. \tag{23}$$

The Wigner function mimics a classical distribution, e.g., the density is recovered by

$$\rho(x) = \frac{1}{2\pi}\int_{-\infty}^{\infty} f(x,k)\,dk, \tag{24}$$

but the non-local features of quantum mechanics are made manifest in the kets $|x \pm y\rangle$ on which $\hat{\rho}$ operates. Because of the infinite barriers, the integration region of Eq. (23) must be bound such that $|x \pm y| \le L/2$. This imposes the restriction $-L/2 + |x| \le y \le L/2 - |x|$. As a result of Eqs. (23) and (A3), the definition of $\psi_k(x)$, and the symmetry of the integrand of Eq. (23) with respect to $y \to -y$, it follows:

$$\begin{aligned} f(x,k) &= \frac{2}{L^2}\sum_{n=1}^{N}(N^2-n^2)\int_{-\Delta}^{\Delta} W_n(k;x,y)dy, \\ W_n(k;x,y) &= \cos(2ky)\sin[k_n(x+y)]\sin[k_n(x-y)], \end{aligned} \tag{25}$$

where $\Delta = (L/2) - |x|$. Observe that closed boundary conditions and the aforementioned discussion entails that $f(x,k) = f(x,-k)$, although that will not hold for open boundary condition situations where current may flow. Introduce $\phi_\pm = 2(k \pm k_n)\Delta$, $\phi_o = 2k\Delta$, and $\mathrm{sinc}(\phi) = (\sin\phi)/\phi$. With $2\sin(a+b)\sin(a-b) = \cos(2b) - \cos(2a)$, then two integrals arise from the integral in Eq. (25) and are

$$\begin{aligned} \int_{-\Delta}^{\Delta}\cos(2ky)\cos(2k_n y)dy &= \Delta\{\mathrm{sinc}(\phi_+) + \mathrm{sinc}(\phi_-)\}, \\ \int_{-\Delta}^{\Delta}\cos(2ky)\cos(2k_n x)dy &= 2\Delta\cos(2k_n x)\mathrm{sinc}(\phi_o), \end{aligned} \tag{26}$$

which results in an analytic relation for $f(x,k)$. If the first integral and second integral of Eq. (26) are denoted $P_n(k,x)$ and $Q_n(k,x)$, respectively, then

$$f(x,k) = \frac{1}{L^2}\sum_{n=1}^{N}(N^2-n^2)\{P_n(k,x) - Q_n(k,x)\}. \tag{27}$$

Recalling the discussion following Eq. (9), the inclusion of $2n_s - 1$ delta function potentials within a well region defined by $-L/2 < x < L/2$ (implying $2n_s$ smaller well-like regions) would alter Eq. (27) by eliminating contributions where n is a multiple of n_s.

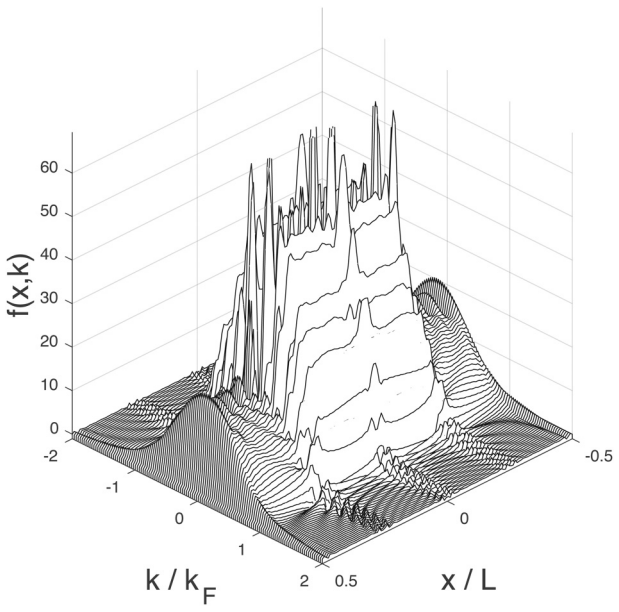

FIG. 2. Wigner function $f(x,k)$ for $N/n_s = n_l = 6$, $n_s = 2$ ($2n_s - 1 = 3$ equi-spaced δ-potentials). $f(x,k)$ is symmetrical across the $x = 0$ and $k = 0$ axes.

For example, $n_s = 2$ as in Fig. 2 (see also Fig. 3) shows four such regions. The formulation has similarities to, but is not the same as a delta-function Krönig-Penny model,[40] because in the present formulation, the boundary conditions are *not* open and therefore there is no current flow.

The density $\rho(x)$ in Eq. (24) is obtained by summing over k_n, resulting in Fig. 3: observe the recovery of the density profile of the ($n = 6$) line of Fig. 1 and that it is repeated in each of the four quadrants, even though the underlying $f(x,k)$ is very different in

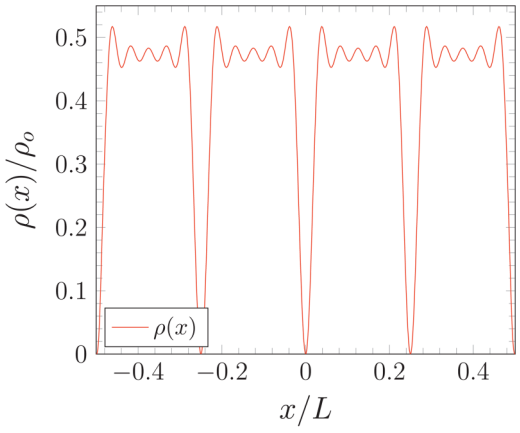

FIG. 3. $\rho(x)$ [Eq. (24)] with $f(x,k)$ from Fig. 2 ($n_l = 6$, $2n_s - 1 = 3$ δ-potential barriers). Compare Fig. 12 in Appendix B.

each of them. Just as $\rho(x)$ is the density in x-space, $\rho(k)$, defined by

$$\rho(k) = \int_{-L/2}^{L/2} f(x, k)dx \tag{28}$$

is the probability density in k-space. Its behavior is contrasted in Fig. 4 to $[1 - (k_j/k_F)^2]$ from the discrete analog of the supply function $f(k)$ of Eq. (A1). The presence of the delta-function barriers results in sharpened regions where $\rho(k)$ is significant, with the sharpened areas corresponding to the k_n of the discrete coefficient in Eq. (27). Increasing the number $2n_s - 1$ of δ-potential barriers within the well serves to sharpen the $\rho(k)$ peaks.

The behavior of $f(x, k)$ visible near the box edges at $\pm L/2$ possesses the same ripples found in the numerical simulation of resonant tunneling diodes (RTDs) (e.g., Fig. 12 of Ref. 41 and Fig. 10 of Ref. 42). Such ripples affect a trajectory interpretation. The region closest to $x = \pm L/2$ is of most interest: those boundaries shall be made finite to analyze effects of a sudden transition.

Observe that the successful development of an analytic solution underscores a difficulty in time-dependent WDF simulations treating a sudden change in which the determination of the WDF relies on incoming boundary conditions[31,41,43] (other Wigner-based methods for treating RTDs exist[33]): the finite difference operator approximating derivatives at the incoming (open) boundary assumes that the boundaries are a thermal Fermi-Dirac distribution (much like the supply function of field emission[44]), but that approximation is undercut by Figs. 4 and 5. That approximation is not correct in the absence of scattering mechanisms that thermalize the distribution far from the RTD. The gradient $\partial_x f(x, k)$ does not vanish at the incident boundaries as assumed, and the oscillations visible for $k > k_F$ depart from $f_o(k) \propto \ln(1 + \exp[\alpha(k_F^2 - k^2)])$ with $\alpha = \hbar^2/2mk_BT$ characteristic of a supply function. The consequences of those approximations are made visibly apparent by simulating an open boundary with an infinite barrier at the origin. The WDF is then symmetrical so that the outgoing boundary is the same as the incoming. Using the thermal distribution at the in/out boundary and numerically solving for the WDF returns an $f(x, k)$ that for small k is noticeably different than the analytical result.[45] Employing the boundary conditions suggested by Fig. 5 would likely correct such deficiencies and have consequences for the RTD simulations as well when $L/2$ is comparable to a scattering mean free path.

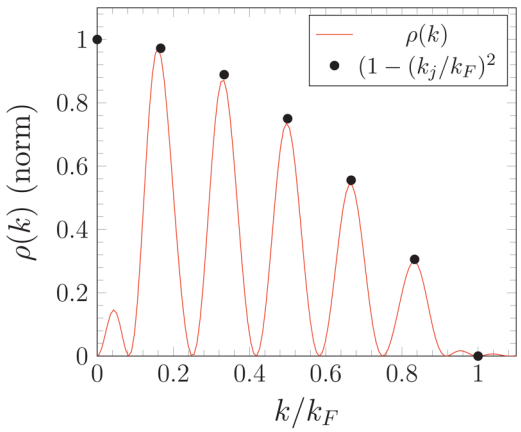

FIG. 4. $\rho(k)$ [Eq. (28)] with $f(x, k)$ from Fig. 2 ($n_l = 6$ levels and $2n_s - 1 = 3$ δ-potential barriers). A $j = 0$ point of $k_j = 2\pi j/n_l$ is shown for visual completeness, but does not correspond to an energy level.

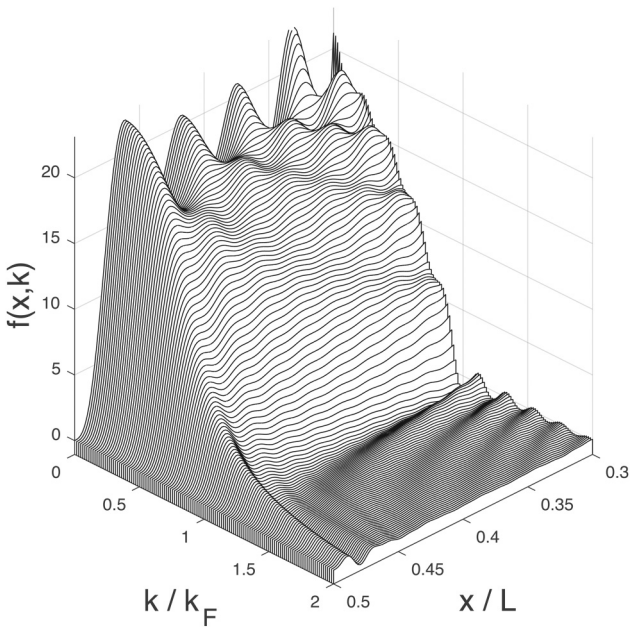

FIG. 5. Close-up of Fig. 2 showing the region nearest $x = L/2$ but not encompassing a Dirac delta potential.

C. Steady state trajectories

The behavior of $f(x, k)$ near $x = L/2$ in closeup accentuates features analogous to those seen in the numerical simulation of resonant tunneling diodes[31,41,42] and field emission[46] using Wigner functions. Contours of $f(x, k)$, which will be associated with a trajectory interpretation,[43] are shown in Fig. 6 and show that some trajectories pass through the entire region of the box. The k values for these trajectories are related to the positions of the peaks in Fig. 5. The relation between the contour lines and trajectories is established by considering the time evolution of the Wigner function, given by

$$\frac{\partial}{\partial t} f(x, k, t) = -\frac{\hbar k}{m}\frac{\partial}{\partial x} f(x, k, t) + \int_{-\infty}^{\infty} V(x, k - k') f(x, k', t)dk', \tag{29}$$

$$V(x, k - k') = -\frac{i}{\pi\hbar}\int_{-\infty}^{\infty} e^{2i(k-k')y} \times \{V(x + y) - V(x - y)\}dy, \tag{30}$$

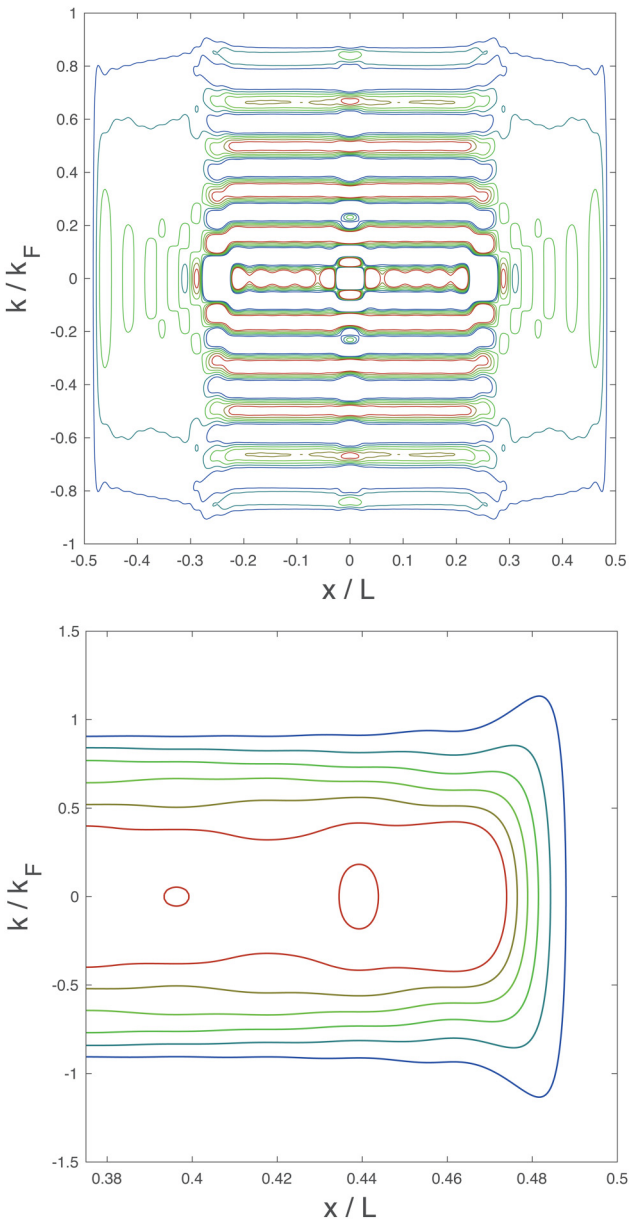

FIG. 6. (*Top*) Contours ($n_l = 6$) equispaced contour lines associated with the full $f(x, k)$ for $n_l = 6$ levels and $2n_s - 1 = 3$ δ-potential barriers. (*Bottom*) Close-up showing the region nearest the "surface" at $x = L/2$: the closest δ-potential is past the left boundary, at $x/L = 0.25$.

which can be recast as $\partial_t f = \mathbb{L} \cdot f$, where the Liouville operator $\mathbb{L}$ is such that

$$f(x, k, t + \delta t) = \exp(i\mathbb{L}\delta t/\hbar) f(x, k, t). \tag{31}$$

The relation to the trajectories of classical phase space $f_c(x, t)$ dictated by

$$\partial_t f_c + \dot{x}\partial_x f_c + \dot{k}\partial_k f_c = 0 \tag{32}$$

can be made if $\dot{x}$ and $\dot{k}$ are defined by the relation to Eq. (29).[31,43] As an example, the harmonic oscillator at a particular energy level has contours of $f(x, k)$ that correspond to constant energy. "Quantum trajectories" can be similarly described for time-independent $f(x, k)$ by their relation to the contour lines. A tunneling time can be related to the trajectories that penetrate barriers of finite size, but such WDFs are more complex than the simple well with infinite walls model.

Consider, therefore, a model of barrier penetration by allowing a finite magnitude wall on only one side. The steady state trajectories associated with in Fig. 5 are shown in Fig. 6. The phase space points (x_j, k_j) on the trajectories can be used to find time by

$$t_{j+1} = t_j + \left(\frac{2m}{\hbar}\right)\frac{x_{j+1} - x_j}{k_{j+1} + k_j}. \tag{33}$$

By comparison, a classical trajectory would have $k_j = k_{initial}$ for all j. The trajectories for the blue, aqua, green, and red trajectories of Fig. 6 (bottom) can thereby be compared: doing so results in Fig. 7, where $x(t)/L$ is compared to t/Δ with $\Delta = mL^2/\pi\hbar n$ and $k_F = 2\pi n/L$, e.g., $\Delta = 46$ fs for $L = 10$ nm and $n = 6$. Also shown are conventional, or "classical," trajectories (dashed lines) where the velocity $\hbar k/m$ is constant and the trajectory does not turn around until the particle is reflected from the wall (top of figure). A noticeable difference is that the WDF trajectories are reflected before they reach the wall.

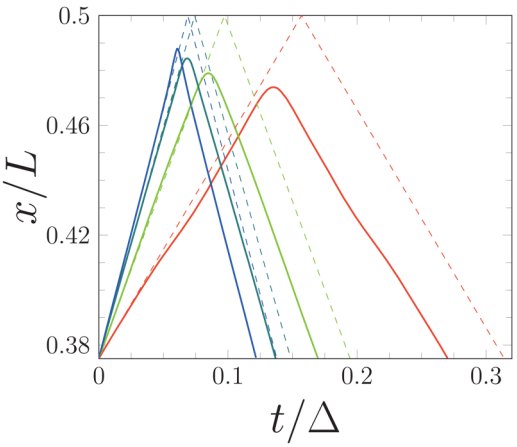

FIG. 7. Trajectories associated with the contours of Fig. 6 (bottom), matched to color. Time is in units of $\Delta = mL^2/\pi\hbar n$. Dashed lines are "classical" trajectories.

III. WELL AND FINITE BARRIER

A. Density

As anticipated in Appendix B, the simplest modification to the well of Sec. II is to retain the infinite potential (either delta function or barrier) at $x = -L/2$ but replace the infinite barrier at $x = 0$ with a finite potential $V(0 \le x < L/2) = \hbar^2 k_o^2/2m$ and retain $V(x \ge L/2) = \infty$. The matrix equation at $x = 0$ that replaces Eq. (11) becomes

$$\begin{bmatrix} 1 & 1 \\ ik & -ik \end{bmatrix} \begin{bmatrix} A_1 \\ B_1 \end{bmatrix} = \begin{bmatrix} 1 & 1 \\ \kappa & -\kappa \end{bmatrix} \begin{bmatrix} A_2 \\ B_2 \end{bmatrix} \tag{34}$$

and the vanishing of the wave function at the boundaries $x = \pm L/2$ result in

$$B_1 = -A_1 e^{-ikL}; \quad A_2 = -B_2 e^{-\kappa L}. \tag{35}$$

The non-vanishing penetration of the wave function in region 2 ($x > 0$) and the vanishing of the wave function at $x = \pm L/2$ require that k_n now becomes

$$k_n \equiv \frac{2\pi}{L}(n - s_n), \tag{36}$$

where s_n is determined by the relation

$$\frac{\tan(k_n L/2)}{k_n} = -\frac{\tanh(\kappa_n L/2)}{\kappa_n} \tag{37}$$

and where $\kappa_n = \sqrt{k_o^2 - k_n^2}$. The determination of s_n is accomplished by numerical means based on the Newtonian iteration for conditions where $k_F < k_o$. For example, for $k_o = 24\pi/L$ with $L = 5$, an approximation finds $s_n \approx 0.01(0.0505n^2 + 2.3648n + 0.2249)$ to 2% accuracy.

By numerical means, s_n is found accurately and k_n constructed from Eq. (36). The wave function is then

$$\begin{aligned} \psi_n(x < 0) &= -2ie^{i\pi s_n} \sin[\pi s_n - k_n x], \\ \psi_n(x > 0) &= -2ie^{-ik_n L/2} \sin(Lk_n/2) \\ &\quad \times \frac{\sinh[\kappa_n x - L\kappa_n/2]}{\sinh(\kappa_n L/2)}. \end{aligned} \tag{38}$$

The normalization N_n is such that

$$N_n^2 = \frac{1}{L}\int_{-L/2}^{L/2} |\psi_n(x)|^2 \, dx = N_l^2 + N_r^2 \tag{39}$$

and makes use of separate integrations over the *left* ($x < 0$) and *right* ($x > 0$) regions such that

$$N_l^2 = 1 + \frac{\sin(2\pi s_n)}{k_n L}, \tag{40}$$

$$N_r^2 = \frac{[\sinh(\kappa_n L) - \kappa_n L]}{4\kappa_n L}\left[\frac{\sin(k_n L/2)}{\sinh(\kappa_n L/2)}\right]^2. \tag{41}$$

The effects of penetration of $\psi_n(x)$ into the barrier are then seen by comparison to the densities of Fig. 1 in Fig. 8, for which the barriers are infinite, using the generalization of Eq. (21) and $\langle x|n\rangle = \psi_n(x)$ but now with k_n dictated by Eq. (36). The impact on the tunneling trajectories for a tunneling barrier of finite magnitude does not admit of an analytic solution of a simplicity comparable to Eq. (27), and so shall be considered by numerical means in a separate study.

B. Evolution after abrupt potential change

The temporal response of the wave function after an abrupt change is possible after the eigenstates of the initial and final conditions are established. If $|\psi_o\rangle$ is the initial wave function, then after an abrupt change, the wave function $|\psi(t)\rangle$ after a time t is given by

$$|\psi(t)\rangle = \sum_{j=1}^{\infty} e^{-i\omega_j t} C_j |j\rangle, \tag{42}$$

where $C_j \equiv \langle j|\psi_o\rangle$, $\hbar\omega_j = \hbar^2 k_j^2/2m$, and $|j\rangle$ are the eigenstates of the system after the change. The initial state $|\psi_o\rangle$ is a combination of initial eigenstates $|n_o\rangle$ encountered in Eq. (22), but now with an "o"-subscript to distinguish them from $|j\rangle$. Specification of the final states $\langle x|n\rangle$ by $\psi_n(x)$ of Eq. (38) after the determination of the values of s_n is numerically possible (and shall be considered in a separate study), but for the present, consider instead a final state that allows for an analytic form without the need to search for s_n. Let the initial state before a sudden change be eigenstates of $V(-L/2 < x < 0) = 0$ and infinite otherwise, and the final state to be eigenstates of $V(-L/2 < x < L/2) = 0$ and infinite otherwise: such a circumstance would correspond to either a single Dirac delta potential at the origin with only the left cell occupied followed by the removal of the Dirac delta potential, or a sudden reduction of

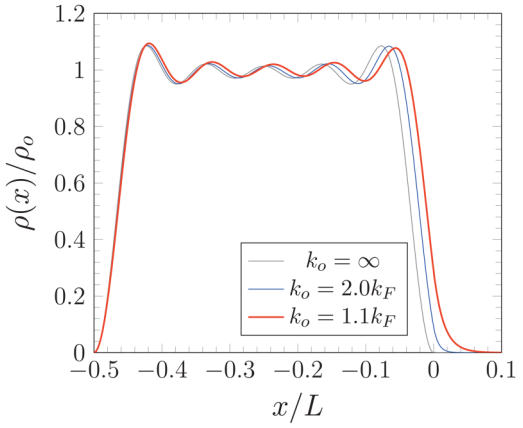

FIG. 8. $\rho(x)/\rho_o$ for $N = 6$ for an infinite barrier at $x = 0$ ($k_o = \infty$, gray), a high barrier ($k_o = 2k_F$, blue), and a low barrier ($k_o = 1.1k_F$, red), where $k_F = k_N$.

the right barrier to zero in the region $0 < x < L/2$: the eigenfunctions for the initial states of both are the same.

More importantly, for the model, the final states over the entire region of size L are analytic and characterized by having twice as many possible energy levels compared to the initial state: in addition to the sin wave functions of the initial state, now the cosine wave functions [corresponding to $k_n = \pi(2n-1)/L$] are allowed. The overlap between the initial and final state wave functions then enables finding C_j. Clearly, $|\psi_o\rangle$ can be constructed as a weighted sum of $|n_o\rangle$ [see Eq. (22)], by

$$|\psi_o\rangle = \sum_{n=1}^{N} \sqrt{f_n}|n_o\rangle. \tag{43}$$

Consequently, the factors $C_{jn} \equiv \langle j|n_o\rangle$ are needed and straightforward to evaluate. Using

$$\begin{aligned} \langle x|n_o\rangle &= 2\sin(2\pi nx/L)\,\Theta(x+L/2)\,\Theta(-x), \\ \langle x|2j\rangle &= \sqrt{2}\sin(2\pi jx/L)\,\Theta[(L/2)^2 - x^2], \\ \langle x|2j-1\rangle &= \sqrt{2}\cos[\pi(2j-1)x/L]\,\Theta[(L/2)^2 - x^2], \end{aligned} \tag{44}$$

then

$$C_{2j,n} = \frac{1}{\sqrt{2}}\,\delta_{jn}, \tag{45}$$

$$C_{2j-1,n} = \frac{4\sqrt{2}n}{\pi\left[(2j-1)^2 - 4n^2\right]}, \tag{46}$$

where δ_{jn} is the Kronecker delta function. Observe, first, that $\sum_{j=1}^{\infty} C_{j,n}^2 = 1$, and second, that after the sudden change in the potential, 50% of the state remains in the initial state $|n_o\rangle$ (that is, $C_{2n,n}^2 = 1/2$) and $\sim 40\%$ in the nearest adjacent states $(C_{2n-1,n}^2 + C_{2n+1,n}^2 \approx (4/\pi^2)(1 + (3/16(\pi n)^2) > 0.41)$ that become available after the potential change.

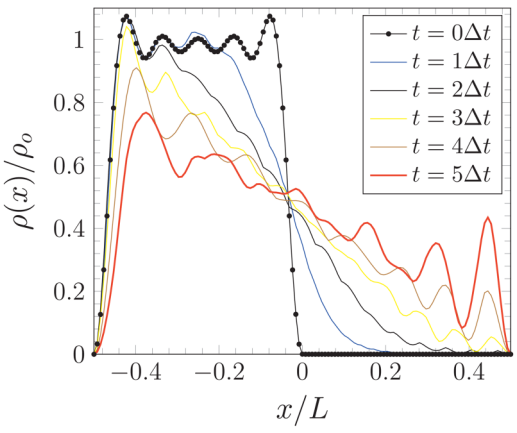

FIG. 9. First six steps in time evolution of $|\psi_o\rangle$ after a sudden change in potential $V(0 < x < L/2) \to 0$ for $N = 6$, in units where $\omega_n \Delta t = n^2\pi/128$.

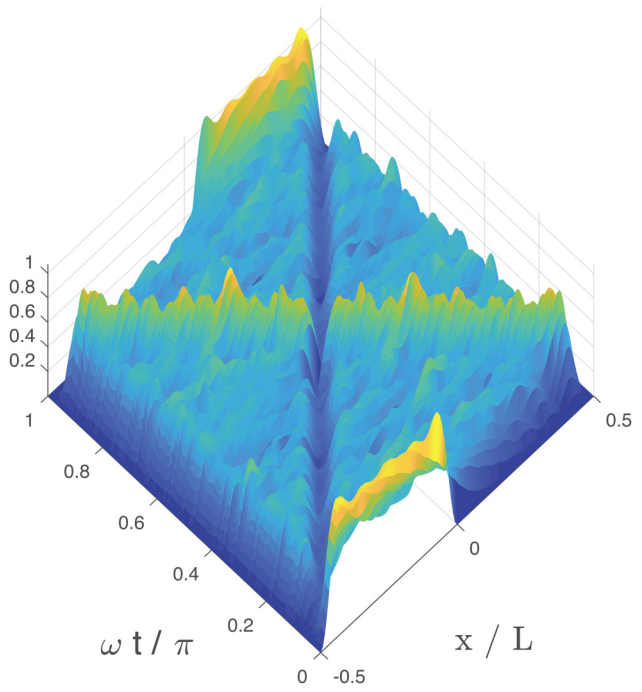

FIG. 10. Behavior of $\rho(x, t)$ from $\omega t = 0$ to $\omega t = \pi$ for $N = 6$. The initial state is shown for $t = 0$ along the $\hat{x}$-axis. The accumulation apparent in Fig. 9 is evident on the right-most corner.

The time evolution of $\psi_o(t)$ for $N = 6$ as per Eq. (43) is shown after a sudden change in potential $V(x) = \infty \to 0$ for $(0 < x < L/2)$ in Fig. 9. The units are chosen such that $\Delta x = L/128$ and $\Delta t = mL^2/256\pi\hbar$. As expected, the density moves

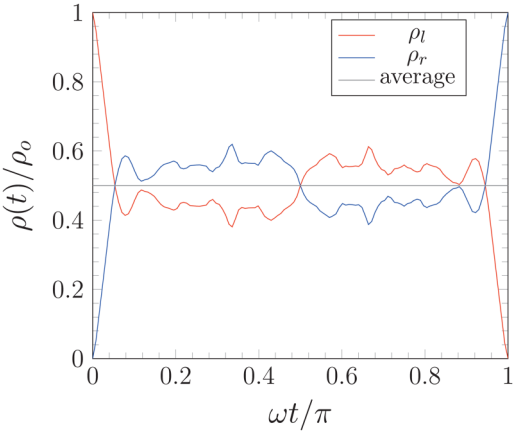

FIG. 11. Left-side and right-side densities based on ρ_l and ρ_r (see text) showing a preponderance or decline in density as a consequence of the migrating depletion and accumulation regions in Fig. 10.

into the unoccupied space for $x > 0$, but perhaps surprisingly, an accumulation builds rapidly near $x \approx L/2$. The rapidity with which this accumulation appears increases with increasing N. If each time slice is stacked, a three dimensional representation of $\rho(x, t) = |\psi(x, t)|^2$ can be created to further examine the behavior of the accumulation. A representation for $N = 6$ is shown in Fig. 10. The perspective reveals that just as an accumulation appears near $x \approx L/2$ for short times, so too does a depletion appear near $x \approx -L/2$, with both the depletion center and the accumulation center migrating to the middle over time.

The behavior can also be considered by looking at the left side density $\rho_l = L^{-1}\int_{-L/2}^{0}\rho(x, t)dx$ compared to the right side density $\rho_r = L^{-1}\int_{0}^{L/2}\rho(x, t)dx$, as shown in Fig. 11: the net positive or negative values of density away from $\omega t = 0$ and $\omega t = \pi$ are a reflection of where the accumulation peak and depletion trough appear in Fig. 10. After a time $t = 2\pi/\omega$, the initial conditions would be recovered: in physical systems, however, scattering processes will act to thermalize the distribution. Modeling those effects, and the consequences for the trajectory model, will be taken up separately.

IV. SUMMARY

The evaluation of Wigner trajectories is made possible using analytic wave functions associated with 1D wells with infinite barriers and delta function barriers. For such simple systems, the Wigner function is analytic and the trajectories easily associated with the contour lines of $f(x, k)$, thereby allowing tunneling times to be evaluated from $\dot{x}$ and $\dot{k}$ on the trajectory lines. Modifications to the wave functions associated with multiple delta function barriers, and with a finite rightmost barrier, are given. The effects on density $\rho(x)$ are shown. The analytical model allowed for the consideration of the consequences of a sudden potential change wherein the region between $0 < x < L/2$ becomes accessible: the behavior of $\rho(x, t)$ was shown and gave rise to accumulation and depletion ridges that migrated symmetrically over the course of time; the analytic nature of the model will allow trajectories for the time dependent conditions to be undertaken. The methods are to be used on more realistic barriers associated with field and photoemission using TMA methods.

ACKNOWLEDGMENTS

The authors gratefully acknowledge support by the Air Force Office of Scientific Research (AFOSR) through the lab task 18RDCOR016, Cathode Materials Research for High Power Microwave Sources. J.L.L. was supported by AFOSR under Award No. FA9500-16-10037.

APPENDIX A: DENSITY

The zero temperature supply function $f(k_x)$ is obtained from the zero-temperature Fermi-Dirac distribution $f_{FD}(E) = \Theta(\mu - E)$, where $\Theta(s)$ is the Heaviside step function, via

$$f(k_x) \equiv \frac{2}{(2\pi)^2}\int dk_y dk_z f_{FD}(E_k) = \frac{1}{2\pi}(k_F^2 - k_x^2), \tag{A1}$$

where $\mu = \hbar^2 k_F^2/2m$. Henceforth, the subscript x is ignored so that $k_x \to k$ and a one-dimensional treatment is recovered. Integrating over $f(k)$ gives the well-known zero-temperature density relation[47]

$$\rho_o = \frac{1}{2\pi}\int_{-k_F}^{k_F} f(k)dk = \frac{k_F^3}{3\pi^2}. \tag{A2}$$

Recovering ρ_o in a discrete formulation makes use of the length of the enclosing box being L and normalized wave functions $\psi_k(x) = \sqrt{2/L}\sin(kx)$ such that the integral of $|\psi_k(x)|^2$ over that box gives unity. Converting the integral in Eq. (A2) to a series makes the replacements: (i) $f(k) \to (k_F^2 - k^2)/(2\pi)$, (ii) $k \to 2\pi j/L$, (iii) $k_F \to 2\pi n/L$, and (iv) $dk \to \Delta k = (2\pi/L)\Delta j$ to obtain

$$d\rho = \frac{1}{2\pi}f(k)dk\int_{-L/2}^{L/2}|\psi_k(x)|^2 dx \to \frac{2\pi}{L^3}(n^2 - j^2)\,\Delta j. \tag{A3}$$

Therefore, with $\Delta j = 1$,

$$\frac{1}{\rho_o}\int d\rho \approx \frac{3L^3}{8\pi n^3}\sum_{j=-n}^{n}\frac{2\pi}{L^3}(n^2 - j^2) = 1 - \frac{1}{4n^2}. \tag{A4}$$

Observe that because the integrand is quadratic in k, the integral and the series representation are identically equal if derivatives at the endpoints of integration (the Euler-MacLauren method) are included: that is, if $g(x)$ is quadratic in x and $g(a) = g(b) = 0$, then

$$\int_a^b g(x)dx = \Delta x\sum_{j=1}^{n} g(x_j) + \frac{\Delta x^2}{12}[g'(a) - g'(b)], \tag{A5}$$

where $g' = dg/dx$, $a = x_1$, and $b = x_n$. The inclusion of the second, or derivatives, term would eliminate the $1/4n^2$ in Eq. (A4). Because energy levels are finely spaced for even micro-scale boxes, n is large and so the $1/4n^2$ term is treated as negligible (e.g., for $\mu = 1.5$ eV, then $n = 1000$ and $1/4n^2 = 2.5 \times 10^{-7}$ for $L = 1\,\mu$m, or $n = 10$ and $1/4n^2 = 0.0025$ for $L = 10$ nm) .

APPENDIX B: STEP FUNCTION BARRIER

The simple problem of reflection and transmission for a step function barrier of height $V_o = \hbar^2 k_o^2/2m$ beginning at $x = 0$ has solutions which are summarized here.[35] The wave function $\psi_k(x)$ with $E = \hbar^2 k^2/2m$ is

$$\psi_k(x < 0) = e^{ikx} + r(k)e^{-ikx}, \tag{B1}$$

$$\psi_k(x \geq 0) = t(k)e^{i\sqrt{k^2 - k_o^2}\,x}. \tag{B2}$$

When $E < V_o$, the coefficients $r(k)$ and $t(k)$ are given by

$$r(k) = -\frac{\kappa + ik}{\kappa - ik}, \tag{B3}$$

$$t(k) = -\frac{2ik}{\kappa - ik} \tag{B4}$$

for $\kappa^2 = k_o^2 - k^2 > 0$. When the barrier is infinite ($V_o \to \infty$), then $\psi_k(x) = \sqrt{2/L}\sin(kx)$ after normalization to a box of length L. It follows that the electron density for the infinite barrier result behaves as

$$\rho(x) = \rho_o\left(1 + 3\frac{\cos\xi}{\xi^2} - 3\frac{\sin\xi}{\xi^3}\right), \tag{B5}$$

where $\xi = 2k_F x$. When V_o is finite, then $r(k < k_o)$ can be expressed as

$$r(k) = -\exp[2i\varphi(k)], \tag{B6}$$

$$\sin(2\varphi) = \frac{2k\kappa}{k_o^2}. \tag{B7}$$

Letting $\varphi = kx_o(k)$, then for small k, $x_o \approx 1/k_o$ is approximately constant to leading order. Letting $r \approx \exp(2ikx_o)$ with $x_o = 1/k_o$ in Eq. (B1) results in the density $\rho(x)$ being of the same form as Eq. (B5) but with the replacement

$$\xi \to 2k_F(x - x_o). \tag{B8}$$

In other words, the density acts as though it has been shifted by an amount x_o as in Fig. 12.

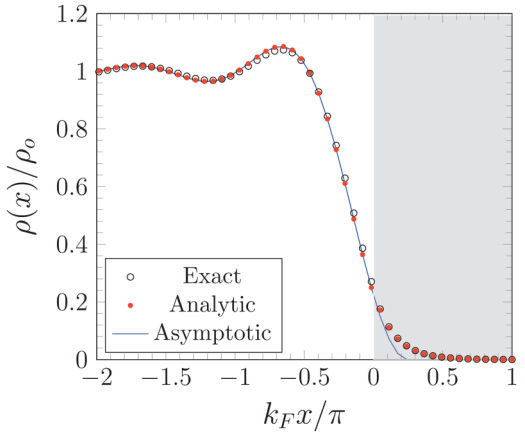

FIG. 12. Density for the infinite barrier compared to density for the finite barrier, with $\rho_o = k_F^3/(3\pi^2)$. "Exact" uses Eq. (B3) for N contributing wave functions; "Analytic" uses $\varphi = kx_o$ in Eq. (B6) for the same N wave functions; and "Asymptotic" uses Eq. (B5) with $\xi \to 2k_F(x - x_o)$ for which the summation over wave functions is done by integration. Compare to Fig. 1.

APPENDIX C: TRIANGULAR BARRIER USING AIRY FUNCTIONS

Through the introduction of $F = q|\mathcal{E}|$, $f = 2mF/\hbar^2$, $k^2 = 2mE/\hbar^2$, and $k_o^2 = 2mV_o/\hbar^2$, Schrödinger's equation becomes[35]

$$-\partial_x^2\psi_k(x) + \left(k_o^2 - k^2 + sfx\right)\psi_k(x) = 0, \tag{C1}$$

where $s = \pm 1$ denotes the sign of the field (e.g., $V_o - Fx = (\hbar^2/2m)(k_o^2 + sfx)$ for $s = -1$). Keep κ strictly positive by defining it by $\kappa^2 \equiv |k_o^2 - k^2|$ and let c^2 denote the sign of $k_o^2 - k^2$ and $(c\kappa)^2 = k_o^2 - k^2$. With $z(x) \equiv (\kappa^2 + sfx)/c^2 f^{2/3}$ then Schrödinger's equation becomes

$$\frac{\partial^2}{\partial_z^2}\psi - c^2 z\psi = 0, \tag{C2}$$

which is Airy's differential equation with solutions $\psi(z) = a\mathrm{Ai}(c^2 z) + b\mathrm{Bi}(c^2 z)$ for $z > 0$. The parameter c (not to be confused with the speed of light) controls the behavior with $c^2 = 1$ and tunneling (under the barrier) occurs, whereas for $c^2 = -1$, flyover (over the barrier) occurs. The simplicity of the simple triangular barrier allows for the usage of $\mathrm{Ai}(c^2 z)$ and $\mathrm{Bi}(c^2 z)$ directly, but a more general formulation for multiple segments uses $\mathrm{Zi}(c, z)$ functions defined in terms of the Airy functions, for which $c = \pm 1$, $\pm i$ denotes the particular Zi.

Restrict attention to the tunneling regime $k^2 < k_o^2$ (or $c^2 = 1$) for a triangular field emission barrier (or $s = -1$). Matching wave function and first derivative, the transmission and reflection coefficients for the simple triangular barrier potential on the introduction of

$$\mathrm{Si}(z) \equiv \mathrm{Ai}(z) - i\mathrm{Bi}(z), \tag{C3}$$

$$|\mathrm{Si}(z)|^2 = \mathrm{Ai}(z)^2 + \mathrm{Bi}(z)^2, \tag{C4}$$

and similarly for $|\mathrm{Si}'(z)|^2$, becomes

$$t(k) = \frac{2k}{k\mathrm{Si}(z) + if^{1/3}\mathrm{Si}'(z)}, \tag{C5}$$

$$r(k) = \frac{k\mathrm{Si}(z) - if^{1/3}\mathrm{Si}'(z)}{k\mathrm{Si}(z) + if^{1/3}\mathrm{Si}'(z)}. \tag{C6}$$

When $\mathrm{Ai}(z)/\mathrm{Bi}(z) \to 0$, then clearly $|r(k)| \to 1$. It can be shown that in the $f \to 0$ limit that Eq. (B3) is recovered. Alternately, the reflection probability $R(k) = 1 - D(k)$ is approximately unity when the transmission probability is small, where

$$D(k) = \frac{4kf^{1/3}}{\pi\left\{k^2|\mathrm{Si}(z)|^2 + f^{2/3}|\mathrm{Si}'(z)|^2\right\} + 2kf^{1/3}}, \tag{C7}$$

$$\to \frac{4k\kappa}{k_o^2}\exp\left(-\frac{4\kappa^3}{3f}\right), \tag{C8}$$

where the asymptotic form (second equation) is, apart from dimensioned coefficients, of the form of the triangular barrier Fowler-Nordheim equation from field emission.

Returning to the form of $r(k)$, it can be shown from Eq. (C5) that (Chap. 26 of Ref. 35)

$$r(k) \approx \frac{\kappa' - ik}{\kappa' + ik}, \tag{C9}$$

$$\kappa' = \kappa - \left(f/\kappa^2 \right), \tag{C10}$$

which has the same form of Eq. (B3) but for the replacement $\kappa \to \kappa'$. Therefore, results from the step-function solution can be appropriated accordingly, particularly the approximation that the density near the barrier acts as though it too is shifted by an amount $x_o' \approx 1/k_o$ in Eq. (B5), which is independent of field, dependent only on the barrier height V_o and acts like the step function barrier encountered in Appendix B.

REFERENCES

[1]Y. Y. Lau, D. Chernin, D. G. Colombant, and P. T. Ho, Phys. Rev. Lett. **66**, 1446 (1991).
[2]L. K. Ang, W. S. Koh, Y. Y. Lau, and T. J. T. Kwan, Phys. Plasmas **13**, 056701 (2006).
[3]L. K. Ang and P. Zhang, Phys. Rev. Lett. **98**, 164802 (2007).
[4]W. S. Koh and L. K. Ang, Nanotechnology **19**, 235402 (2008).
[5]J.-W. Han, J. S. Oh, and M. Meyyappan, Appl. Phys. Lett. **100**, 213505 (2012).
[6]P. Zhang, A. Valfells, L. K. Ang, J. W. Luginsland, and Y. Y. Lau, Appl. Phys. Rev. **4**, 011304 (2017).
[7]P. Zhang and Y. Y. Lau, J. Plasma Phys. **82**, 595820505 (2016).
[8]P. Kapur and R. Peierls, Proc. R. Soc. Lond. Ser. A **163**, 606 (1937).
[9]C. J. Edgcombe, in *Advances in Imaging and Electron Physics*, edited by P. Hawkes (Elsevier, 2010), Vol. 162, pp. 77–127.
[10]A. Kyritsakis, G. Kokkorakis, J. Xanthakis, T. Kirk, and D. Pescia, Appl. Phys. Lett. **97**, 023104 (2010).
[11]F. Andreas, S. M. Marwan, and G. F. Richard, J. Vac. Sci. Technol. B **31**, 032201 (2013).
[12]K. L. Jensen, D. A. Shiffler, M. Peckerar, J. R. Harris, and J. J. Petillo, J. Appl. Phys. **122**, 064501 (2017).
[13]R. H. Dicke, and J. P. Wittke, *Introduction to Quantum Mechanics* (Addison-Wesley, Reading, MA, 1960), p. 369.
[14]R. Shankar, *Principles of Quantum Mechanics* (Plenum Press, New York, 1980), p. 612.
[15]M. Cahay and S. Bandyopadhyay, *Problems in Quantum Mechanics: For Material Scientists, Applied Physicists and Device Engineers* (John Wiley & Sons, Inc., Hoboken, NJ, 2017).
[16]M. Buttiker, Phys. Rev. B **27**, 6178 (1983).
[17]P. J. Price, Phys. Rev. B **38**, 1994 (1988).
[18]E. H. Hauge and J. A. Støvneng, Rev. Mod. Phys. **61**, 917 (1989).
[19]O. Costin, R. Costin, I. Jauslin, and J. Lebowitz, J. Appl. Phys. **124**, 213104 (2018).
[20]A. Chatziafratis, G. Fikioris, and J. P. Xanthakis, Proc. R. Soc. A **474**, 20170692 (2018).
[21]K. L. Jensen, J. J. Petillo, S. Ovtchinnikov, D. N. Panagos, N. A. Moody, and S. G. Lambrakos, J. Appl. Phys. **122**, 164501 (2017).
[22]H.-W. Lee, Phys. Rep. **259**, 147 (1995).
[23]M. Razavy, Phys. Lett. A **212**, 119 (1996).
[24]S. Dries, B. Fons, and M. Wim, Phys. A Stat. Mech. Appl. **391**, 78 (2012).
[25]J.-P. Vigier, C. Dewdney, P. R. Holland, and A. Kyprianidis, in *Quantum implications: Essays in honour of David Bohm*, edited by B. J. Hiley and F. D. Peat (Routledge, New York, NY, 1987), pp. 169–204.
[26]X. Oriols, F. Martin, and J. Sune, Solid State Commun. **99**, 123 (1996).
[27]K. Na and R. Wyatt, Int. J. Quantum Chem. **81**, 206 (2001).
[28]A. S. Landsman and U. Keller, Phys. Rep. **547**, 1 (2015).
[29]T. Zimmermann, S. Mishra, B. R. Doran, D. F. Gordon, and A. S. Landsman, Phys. Rev. Lett. **116**, 233603 (2016).
[30]K. L. Jensen and F. A. Buot, "Particle trajectory tunneling—A novel approach to quantum transport," in *2nd International Conference on Vacuum Microelectronics* (Institute of Physics, 1989), Vol. 99, pp. 137–140.
[31]F. A. Buot and K. L. Jensen, Phys. Rev. B **42**, 9429 (1990).
[32]Y. Hsu and G. Y. Wu, J. Appl. Phys. **71**, 304 (1992).
[33]D. Querlioz and P. Dollfus, *The Wigner Monte-Carlo Method for Nanoelectronic Devices: Particle Description of Quantum Transport and Decoherence* (Wiley, London, 2010), p. 243.
[34]See, for example, the notation of Problem 7.7 of Ref. 15.
[35]K. L. Jensen, *Introduction to the Physics of Electron Emission* (John Wiley & Sons, Inc., Hoboken, NJ, 2017).
[36]E. Butkov, *Mathematical Physics* (Addison-Wesley, Reading, MA, 1968).
[37]M. Belloni, M. A. Doncheski, and R. W. Robinett, Am. J. Phys. **72**, 1183 (2004).
[38]F. A. Buot, Phys. Rev. B **14**, 3310 (1976).
[39]M. Hillery, R. Oconnell, M. Scully, and E. Wigner, Phys. Rep. **106**, 121 (1984).
[40]See, for example, Ref. 15, in particular, Problems 7.11, 8.3, and 8.4, where resonant transmission occurs.
[41]W. R. Frensley, Rev. Mod. Phys. **62**, 745 (1990).
[42]K. L. Jensen and A. Ganguly, J. Appl. Phys. **73**, 4409 (1993).
[43]K. L. Jensen and F. A. Buot, IEEE. Trans. Electron Devices **38**, 2337 (1991).
[44]E. L. Murphy and R. H. Good, Phys. Rev. **102**, 1464 (1956).
[45]K. L. Jensen, unpublished results (1993).
[46]K. L. Jensen, J. Vac. Sci. Technol. B **13**, 505 (1995).
[47]R. Kubo, *Statistical Mechanics, an Advanced Course With Problems and Solutions* (North-Holland, Amsterdam, 1965).